

Oxyhemoglobin and Cerebral Blood Flow Transients Detect Infarction in Rat Focal Brain Ischemia

Janos Luckl,^{a,b,c} Wesley Baker,^{d,e} Krisztina Boda,^c Miklos Emri,^f Arjun G Yodh^e and Joel H Greenberg^{a*}

^a Department of Neurology, University of Pennsylvania, Philadelphia, USA

^b Department of Neurology, University of Szeged, Szeged, Hungary

^c Department of Medical Physics and Informatics, Szeged, Hungary

^d Department of Neurology, Children's Hospital of Philadelphia, Philadelphia, USA

^e Department of Physics and Astronomy, University of Pennsylvania, Philadelphia, USA

^f Division of Nuclear Medicine and Translational Imaging, Department of Medical Imaging, Faculty of Medicine, University of Debrecen, Debrecen, Hungary

Abstract—Spreading depolarizations (SD) refer to the near-complete depolarization of neurons that is associated with brain injuries such as ischemic stroke. The present gold standard for SD monitoring in humans is invasive electrocorticography (ECoG). A promising non-invasive alternative to ECoG is diffuse optical monitoring of SD-related flow and hemoglobin transients. To investigate the clinical utility of flow and hemoglobin transients, we analyzed their association with infarction in rat focal brain ischemia. Optical images of flow, oxy-hemoglobin, and deoxy-hemoglobin were continuously acquired with Laser Speckle and Optical Intrinsic Signal imaging for 2 h after photochemically induced distal middle cerebral artery occlusion in Sprague-Dawley rats ($n = 10$). Imaging was performed through a 6×6 mm window centered 3 mm posterior and 4 mm lateral to Bregma. Rats were sacrificed after 24 h, and the brain slices were stained for assessment of infarction. We mapped the infarcted area onto the imaging data and used nine circular regions of interest (ROI) to distinguish infarcted from non-infarcted tissue. Transients propagating through each ROI were characterized with six parameters (negative, positive, and total amplitude; negative and positive slope; duration). Transients were also classified into three morphology types (positive monophasic, biphasic, negative monophasic). Flow transient morphology, positive amplitude, positive slope, and total amplitude were all strongly associated with infarction ($p < 0.001$). Associations with infarction were also observed for oxy-hemoglobin morphology, oxy-hemoglobin positive amplitude and slope, and deoxy-hemoglobin positive slope and duration (all $p < 0.01$). These results suggest that flow and hemoglobin transients accompanying SD have value for detecting infarction. © 2022 IBRO. Published by Elsevier Ltd. All rights reserved.

Key words: spreading depolarization, focal brain ischemia, optical imaging, flow transients, hemoglobin transients, histological outcome.

INTRODUCTION

Spreading depolarizations (SD) is the term for the near-complete depolarization of neurons (Somjen, 2001; Dreier, 2011) accompanied by the decrease of membrane resistance (Czeh et al., 1993), the loss of electrical activity

(Leao, 1944), neuronal swelling and distortion of dendritic spines, (Takano et al., 2007) (Risher et al., 2009) and cytotoxic edema (Nicholson et al., 1978; Takano et al., 2007). Furthermore, SD involves astrocytes (Largo et al., 1996; Peters et al., 2003; Chuquet et al., 2007; Urbach et al., 2015), stimulates microglial cells and inflammasome formation, and activates cytokine gene expression (Jander et al., 2001; Walsh et al., 2014). SD is responsible for necrotic and selective neuronal lesion evolution in gray matter as reported in diverse disease models and species (Lauritzen et al., 2011; Hartings et al., 2017). There is a strong clinical experience that SD is associated with brain injuries such as ischemic stroke, subarachnoid hemorrhage, and traumatic brain injury (Dohmen et al., 2008; Hartings et al., 2011; Lückl

*Corresponding author. Address: Perelman School of Medicine, University of Pennsylvania, Philadelphia, PA 19104, USA.

E-mail address: Joel@penntmedicine.upenn.edu (J. H Greenberg).

Abbreviations: CBF, cerebral blood flow; COSBID, Co-Operative Studies on Brain Injury Depolarizations; Deoxy-Hb, deoxy-hemoglobin, LEDs, light emitting diodes; ECoG, electrocorticography; EEG, electroencephalography; LD, laser Doppler; LSI, laser speckle imaging; MCA, middle cerebral artery; OIS, optical intrinsic signal; OR, odds ratios; Oxy-Hb, oxy-hemoglobin; ROI, regions of interest; SD, spreading depolarization; TTC, triphenyltetrazolium chloride.

et al., 2018; Dreier et al., 2022). Accordingly, the Co-Operative Studies on Brain Injury Depolarizations (COS-BID) Group recommends routine monitoring of SD for brain-injured patients (Dreier et al., 2017).

The present gold standard for detection of SD in human is electrocorticography (ECoG) with a linear subdural platinum electrode strip. ECoG, however, has the disadvantage of allowing only invasive measurement of SDs in patients, and it does not provide information on hemodynamic changes. To overcome these challenges, the consensus article of COSBID concludes that the use of non-invasive technologies such as continuous scalp electroencephalography (EEG) and optical hemodynamic imaging (e.g., near-infrared spectroscopy or diffuse correlation spectroscopy) hold promise (Dreier et al., 2017).

In animal models of stroke, the optical techniques of laser Doppler (LD) and laser speckle imaging (LSI) have been used to measure regional cerebral blood flow (CBF) related to SDs (Hossmann, 1996) (Dunn et al., 2001). Additionally, optical intrinsic signal (OIS) imaging enables the measurement of regional oxy-hemoglobin and deoxy-hemoglobin concentrations (Jones et al., 2001), and strong correlations between ECoG changes and LSI/LD/OIS metrics have been demonstrated (Dahlem and Müller, 1997; Peixoto et al., 2001; Obrenovitch et al., 2009; Lückl et al., 2012).

In our work, we sought to investigate whether these cortical hemoglobin and flow transients that accompany SD have value for detecting infarction in a rat focal brain ischemia model. Continuous 2D topographic maps of cortical oxy- and deoxy-hemoglobin were measured with OIS (Grinvald et al., 1986a; Dunn et al., 2003). Corresponding topographic maps of cortical blood flow were measured in parallel with LSI (Dunn et al., 2001). We hypothesized that different parameters (amplitude, durations, slopes and shapes) of the hemoglobin and flow transients captured from these images are associated with infarction. To answer the hypothesis, we analyzed the animals of a prospective study ($n = 10$) with dichotomized histological outcomes. A positive result preclinically motivates future translational research on the development of near-infrared spectroscopy and diffuse correlation spectroscopy biomarkers of injury in humans with ischemic stroke.

EXPERIMENTAL PROCEDURES

Photochemically induced distal middle cerebral artery occlusion

All procedures performed were approved by the Institutional Animal Care and Use Committee of the University of Pennsylvania. Mature, adult male Sprague–Dawley rats ($n = 10$, 290–320 g, ~12–13 weeks of age) were anesthetized with 4% isoflurane for induction in a mixture of 50% nitrous oxide and 50% oxygen and maintained on 1.2–1.3% isoflurane (1.0–1.25 MAC) in 70% nitrous oxide and 30% oxygen during surgery and throughout the study. Body temperature was monitored by a rectal probe and maintained at 37.5 ± 0.2 °C with a heating blanket regulated by a

homeothermic blanket control unit (Harvard Apparatus Limited Holliston, MA, USA). A polyethylene catheter (PE-50) was placed into the tail artery for the measurement of arterial blood pressure and for blood gas sampling. Blood pressure was continuously monitored using a pressure transducer and recorded on a computer-based recording system (PowerLab, ADInstruments, Colorado Springs, CO, USA). The right common carotid artery was exposed by a ventral midline incision in the neck and the retraction of the sternocleidomastoid muscle. The exposed artery was surrounded by a snare. Of note, care was taken to avoid trauma to the vagal nerve while dissecting the carotid sheath (this was facilitated by our use of the photochemically induced ischemia model, which only requires the exposure of a short section of the common carotid artery).

The rats were placed into a stereotaxic head holder, and a 6×6 mm area centered 3 mm posterior and 4 mm lateral to Bregma was uniformly thinned to translucency for optical imaging (Fig. 1). To reduce specular reflections, ultrasound gel was applied to the thinned skull and a glass coverslip placed on top. Special attention was paid during surgical preparation to make the skull thickness uniform (Parthasarathy et al., 2008). To induce middle cerebral artery (MCA) occlusion, a 2-cm vertical incision was made midway between the right eye and the right ear. The temporalis muscle was separated and retracted to expose the zygomatic and squamosal bones. Under an operating microscope (Carl Zeiss, Inc.), a burr hole of 4 mm in diameter was made with a high-speed drill 1 mm rostral to the anterior junction of the zygomatic and squamosal bones, revealing the distal segment of the MCA. The epidural temperature was monitored by probe and maintained at 37.5 ± 0.3 °C with a custom-made air delivery blowing warm air on the dura.

The right side of the stereotaxic frame was tilted upward to facilitate the focusing of the beam from a 4 mW diode laser (532 nm wavelength, LaserGlow Technologies, model LRS-0532-KFM-00030–03) on the exposed MCA (a spherical lens of 25 cm focal length

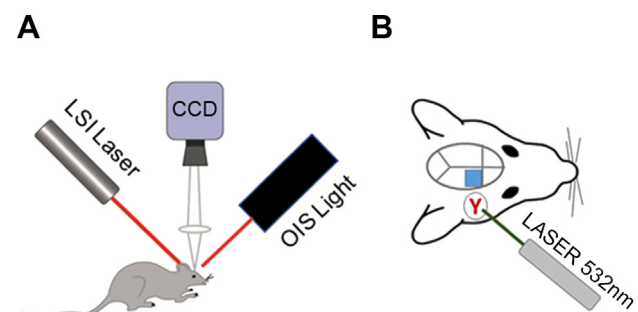


Fig. 1. Experimental setup. (A) Laser Speckle Imaging (LSI) and multispectral Optical Intrinsic Signal (OIS) imaging were used to acquire topographic images (with a CCD camera) of cortical cerebral blood flow (CBF), oxy-hemoglobin (Oxy-Hb), and deoxy-hemoglobin (Deoxy-Hb) once every-two seconds. (B) Diagram of the rat brain showing the 6×6 mm thinned part of the skull for hemodynamic imaging (blue square). Illumination from a laser (532 nm wavelength) produced a thrombus proximally to the Y-shaped juncture of the frontal and parietal branches of the middle cerebral artery.

was used for focusing). A stock solution of Erythrosin B dye (MP Biomedicals, Solon, OH, USA), 17 mg/mL in 0.9% saline, was then injected intravenously (via the tail vein) at a dose of 40 mg/kg.

Immediately after injection of the dye, the MCA was irradiated with the diode laser. The irradiation produced a thrombus proximally to the Y-shaped juncture of the frontal and parietal branches of the MCA. An orange fluorescence was immediately observed in the irradiated distal MCA segment under the operating microscope. A white thrombus began to form approximately 4–5 min later within the fluorescent segment and gradually elongated distally. Following the irradiation, the right CCA was also occluded by tightening the snare.

Changes in oxygenation and blood flow were monitored through the thinned skull preparation with optical intrinsic signal imaging (OIS) (Grinvald et al., 1986b; Kohl et al., 2000) and laser speckle imaging (LSI) (Briers, 2001; Dunn et al., 2001; Durduran et al., 2004).

Cerebral hemodynamic imaging

The techniques of LSI and OIS were combined to longitudinally acquire 2D images of cortical blood flow (CBF), oxy-hemoglobin (Oxy-Hb), and deoxy-hemoglobin (Deoxy-Hb). A schematic of the instruments used to acquire the data is shown in Fig. 1, and technical details of the instrument are described elsewhere (Baker et al., 2013). Note that two sets of illumination sources were used for OIS. For the first five animals imaged, a xenon arc lamp was directed through a filter wheel (Luckl et al., 2010). For the last five animals imaged, OIS illumination was performed with three collimated light emitting diodes (LEDs) (Baker et al., 2013). With this instrument, we sequentially acquired one three-wavelength set of OIS images and 15 LSI images every 2 s.

OIS and LSI imaging was performed from 5-min prior to 2-h after the initiation of MCA occlusion in 15-min-long sequences (there was approximately 10–20 s between the 15-min-long sequences). For LSI analysis, a 7×7 pixel sliding window was employed to calculate speckle contrast images, which were then converted to speckle CBF images based on an assumed Lorentzian velocity distribution of the moving red blood cells (Zhou et al., 2008). To improve SNR, 15 speckle CBF images were averaged to obtain one CBF image every 2 s. Relative CBF was obtained by normalizing the CBF index images by the mean CBF index image during the 5-min pre-occlusion baseline with a correction for biological zero (Zhou et al., 2008).

For OIS, differential changes in Oxy-Hb and Deoxy-Hb relative to their average levels during the first minute after MCA occlusion were computed via the modified Beer-Lambert law (Kohl et al., 2000; Dunn et al., 2003; Baker et al., 2013). (Note, with the modified Beer-Lambert law, computing changes relative to a pre-occlusion baseline is not feasible because the method breaks down for the large hemoglobin decreases that accompany occlusion (Jones et al., 2008)) Finally, a 5-by-5 pixel sliding spatial Gaussian filter was applied to

the relative CBF, Oxy-Hb, and Deoxy-Hb images to improve SNR.

Mapping of infarcted tissue to the LSI and OIS images

Tissue staining with 2% diphenyltetrazolium chloride (TTC) at 24 h after MCA occlusion has been established as an excellent marker of the extent of brain tissue damage (Bederson et al., 1986; Bardutzky et al., 2005). Accordingly, at 24 h after MCA occlusion, the animals were sacrificed.

The brain was removed from the skull and was sectioned in the coronal plane at 1.5-mm intervals using a rodent brain matrix. The brain slices were stained with TTC and photographed, and the cortical infarct volume was determined as described previously (Luckl et al., 2008). The distance between the midline and the border of the infarct zone on the TTC slices was measured and mapped onto the LSI and OIS images individually in each animal (see Fig. 2). Specifically, a high-resolution laser Speckle contrast image (obtained prior to MCA occlusion) was used for the mapping, which clearly showed the blood vessels (Dunn et al., 2001). For the comparison of transients propagating in infarcted versus non-infarcted tissue, nine circular regions of interest (ROI, 0.3 mm in diameter) were used. The Speckle contrast image was divided into nine equal sectors, and one ROI was placed in each sector (see Fig. 2). Six ROIs (i.e., #1–6) were placed in the infarct zone, while the remaining three ROIs (i.e., #7–9) were placed in non-infarcted tissue. Care was taken to ensure the ROIs were not over any large blood vessels.

Analysis of transients

As described in the previous section, transients were identified and characterized from the image data via analysis of nine spatial ROIs (see Fig. 2). Relative CBF, Oxy-Hb, and Deoxy-Hb at each ROI were plotted vs time. The temporal plots were manually reviewed to identify hemodynamic transients.

Transients were identified by their propagating feature (e.g., an increased relative CBF wave seen in at least two ROIs with appropriate time delay). Once identified, transients were categorized as Type I, Type II, or Type III. Type I transients are positive monophasic (have a positive amplitude only), Type II transients are biphasic (have a negative and positive amplitude), and Type III transients are negative monophasic (have a negative amplitude only) (see Fig. 3). Then, for a given ROI, baseline relative CBF, Δ Oxy-Hb, and Δ Deoxy-Hb levels for each transient were determined by taking their mean values across the 5-s window prior to the transient's start. Recall, as described in the Cerebral Hemodynamic Imaging section, relative CBF is the speckle CBF index normalized by its pre-occlusion level; Δ Oxy-Hb and Δ Deoxy-Hb are differential concentration changes relative to the first minute after MCA occlusion in μ M.

For CBF transients of Type I and Type II, the maximum relative CBF levels during the transients were identified. The positive relative CBF amplitude (CBF

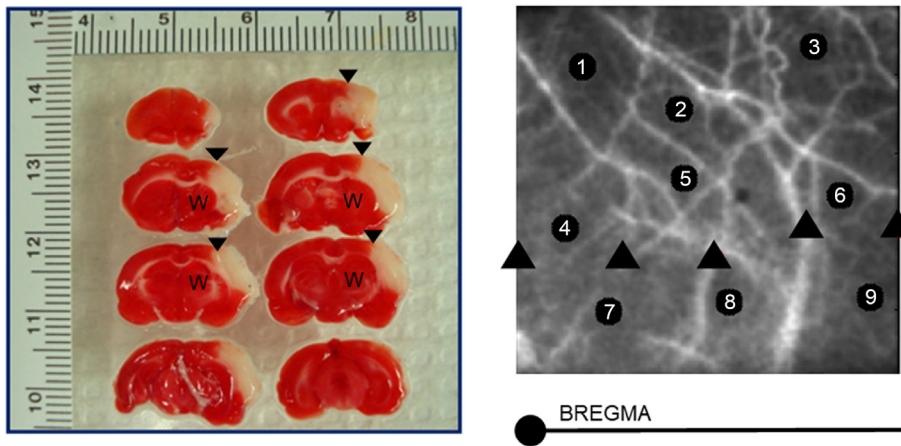


Fig. 2. Mapping the layout of ROIs with the border of the infarcted tissue in a representative animal. Slices of TTC staining can be seen in the left panel. Four slices (4×1.5 mm) marked with the letter “W” are under the 6×6 mm optical imaging window. The black circles depict the positions of each ROI (1–9) on a laser Speckle contrast image (6×6 mm) in the right panel. The black triangles represent the border between the infarcted (ROI 1–6) and non-infarcted territory (ROI 7–9) both on the TTC slices and laser Speckle contrast image. The relative, spatial position of the “optical window” to Bregma and from midline (1 mm) is illustrated below the panel on the right.

PAMP is the difference between the transient’s maximum Δ Oxy-Hb level and its baseline level).

Finally, a TAMP parameter was determined for each transient: for transients of Type I, $TAMP = PAMP$; for transients of Type II, $TAMP = PAMP + NAMP$ (i.e., the peak-to-peak height); and for transients of Type III, $TAMP = NAMP$. In addition, the duration of each transient was determined, which was the difference between the start time and end time of the transient (start and end times were determined by the times at which the signal intercrossed with the ascending and the descending leg of the transient, see Fig. 3). Of note, some transients did not return to their baseline levels at all, while others did not return to their baseline levels by the end the 15-

PAMP) is the difference between the transient’s maximum level and its baseline level. The positive CBF slope (CBF Pslope) is defined as the CBF PAMP divided by the time it takes CBF to reach the CBF PAMP level from its baseline level (see Fig. 3). For CBF transients of Type II and Type III, the minimum relative CBF levels during the transients were identified. The negative CBF amplitude (CBF NAMP) is the difference between the transient’s baseline level and its minimum level. The negative CBF slope (CBF Nslope) is defined as the CBF NAMP divided by the time it takes CBF to reach the CBF NAMP level from its baseline level (see Fig. 3). The PAMP, Pslope, NAMP, and Nslope parameters are defined the same way for Oxy-Hb and Deoxy-Hb transients (e.g., Oxy-Hb

min-long sequence of LSI/OIS acquisition (recall, LSI/OIS imaging was performed in sequential 15-min-long sequences with ~ 10 – 20 s between sequences). For these transients, duration could not be measured.

Statistical analysis

Statistical calculations were performed with SPSS version 26 (IBM Corporation). All statistical tests were 2-sided, and $p < 0.05$ was considered to indicate significance. We assessed whether the CBF transient characterization parameters (i.e., NAMP, PAMP, TAMP, duration, Nslope, Pslope) differed between the infarcted and non-infarcted tissue regions. Specifically, we used a

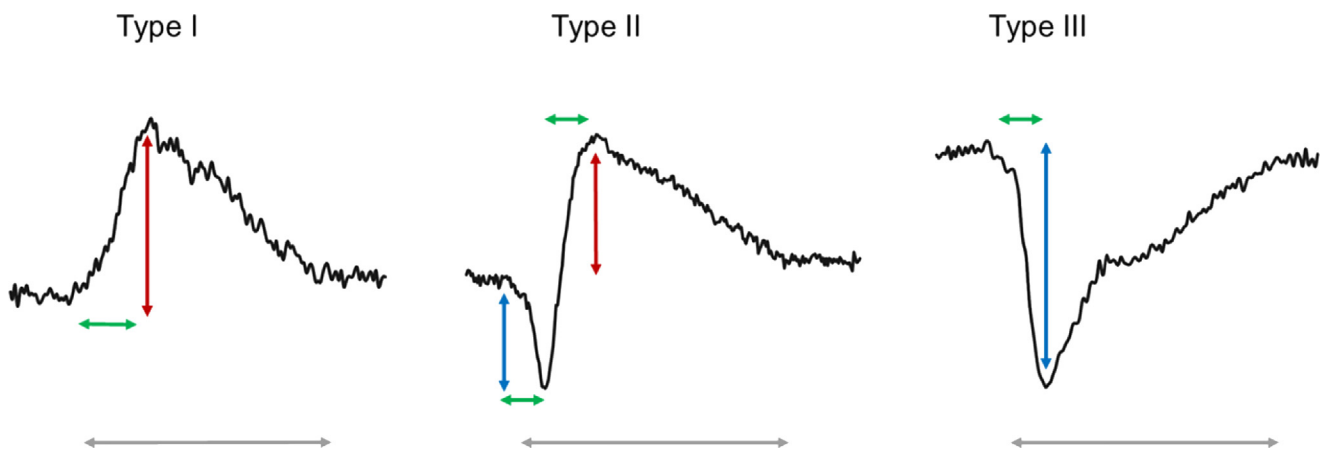


Fig. 3. Representative traces of different types (I, II, III) of transients. The duration (grey line) of the transients were determined as the time at which the average signal intercrossed with the ascending or the descending leg of the transients. The amplitude denotes the peak magnitude change in relative cerebral blood flow (%), oxy-hemoglobin concentration (μ M), or deoxy-hemoglobin concentration (μ M). The negative amplitude (NAMP, blue vertical line) and positive amplitude (PAMP, red vertical line) were measured separately. We also calculated the slope of the positive and negative amplitudes. The positive and negative slopes (Pslope and Nslope) are the amplitudes divided by the preceding temporal durations indicated by the green horizontal lines. Finally, the total amplitude (TAMP) is defined as PAMP, PAMP + NAMP, and NAMP for the type I, II, and III transients, respectively.

mixed-model ANOVA (Brown and Prescott, 1999) to compare the means of these characterization parameters between ROIs in the infarcted tissue (i.e., ROIs #1–6) and ROIs in the non-infarcted tissue (i.e., ROIs #7–9). For each animal, the characterization parameters in each infarcted ROI (i.e., ROIs #1–6) were used as a separate datapoint for infarcted tissue in the comparison. Likewise, the characterization parameters in each non-infarcted ROI (i.e., #7–9) were used as a separate data-point for non-infarcted tissue. The mixed-model ANOVA accounts for the lack of independence across the multiple infarcted and non-infarcted ROIs from each animal. The model further accounts for the lack of independence across multiple transients occurring in the same animal. Mixed-model ANOVA was also used to compare the means of the analogous Oxy-Hb and Deoxy-Hb transient characterization parameters between the infarcted and non-infarcted tissue regions. Finally, the estimated mean and the standard error of the estimated mean obtained from the mixed-model ANOVA is reported for each characterization parameter.

We were also interested in differences between the occurrence frequency of transient types that propagated across infarcted versus non-infarcted tissue. First, we computed the number of each CBF transient type propagating across infarcted tissue as a percentage of the total number of CBF transients (of all types) detected. The analogous percentages for non-infarcted tissue, and for the Oxy-Hb and Deoxy-Hb transients, were also computed. Next, we computed the odds ratios (OR) for infarction of each CBF, Oxy-Hb, and Deoxy-Hb transient type. To assess whether the odds across transient types were significantly different from each other, a generalized mixed logistic regression model with binary matched pairs was used (Brown and Prescott, 1999). The following estimated ratios (with 95% confidence intervals) were obtained from the model: OR (Type III vs Type I) and OR (Type II vs Type I). The mixed logistic regression model accounts for the lack of independence between transients from the same animal.

Summary statistics are presented using means and standard deviations for: 1) the cortical infarct volume; 2) the spatially averaged relative CBF across the infarcted ROIs (#1–6) immediately after MCA occlusion; 3) the spatially averaged relative CBF across the non-infarcted ROIs (#7–9) immediately after MCA occlusion; 4) the number of CBF transients per animal; and 5) the CBF, Oxy-Hb, and Deoxy-Hb transient characterization parameters (i.e., NAmp, PAmp, TAmplitude, duration, Nslope, Pslope) across the non-infarcted and across the infarcted tissue regions.

RESULTS

For all animals ($n = 10$), the physiological variables (blood pressure, blood gas, core and epidural temperature) measured remained within normal ranges for the 2 h of monitoring after MCA occlusion. The average cortical infarct volume across animals was $109 \pm 39 \text{ mm}^3$. CBF, Oxy-Hb, and Deoxy-Hb transients in an exemplar animal are shown in Fig. 4. In total,

across all animals and all nine ROIs, 285 CBF transients, 234 Oxy-Hb transients, and 196 Deoxy-Hb transients were analyzed. Of these totals, the percentages of each transient type in infarcted and non-infarcted tissue regions are reported in Table 1.

Of note, unanticipated transient malfunctions in the OIS instrumentation occurred in two animals, which resulted in the loss of 15 min of OIS data post-occlusion for each animal. During these two intervals of OIS data loss, 16 CBF transients were detected. There were an additional 35 CBF transients for which accompanying Oxy-Hb and Deoxy-Hb transients were not detected. The mismatch rate between the CBF and Oxy-Hb transients was 62% (22/35) over the infarcted area. Finally, for 38 of the detected Oxy-Hb transients, accompanying Deoxy-Hb transients were not detected. The magnitude of the mismatch between the Oxy-Hb and Deoxy-Hb transients proved to be 44% (17/38) over the infarcted area.

Cerebral blood flow and flow transients

Immediately after MCA occlusion, the average relative CBF (fraction of pre-occlusion CBF) in the infarcted and non-infarcted regions were $34 \pm 13\%$ and $51 \pm 11\%$, respectively. As expected, the post-occlusion CBF in the infarcted region was lower ($p < 0.001$). We detected 5.2 ± 2.2 propagating CBF transients per animal. Of the total number of transients analyzed, 48% were in the infarcted tissue, and 52% were in the non-infarcted tissue. The flow transients propagated across tissue in multiple directions. Most transients (71%) propagated from frontal to caudal (either lateral-medial or medial-lateral). The remainder of transients propagated in the reverse direction, i.e., from caudal to frontal.

The PAmp, TAmplitude and Pslope CBF transient characterization parameters were higher in the non-infarcted tissue than the infarcted tissue ($p < 0.001$ for all three parameters) (Table 2, Fig. 5). There was no difference in the other three characterization parameters between non-infarcted and infarcted tissue.

CBF transient type was also associated with infarction ($p < 0.001$). Further, the generalized mixed logistic regression model estimated that the odds of infarction for Type III are 40.6 and 25.0 times higher than the corresponding odds for Type I and Type II, respectively (i.e., OR (Type III vs Type I) = 40.6, OR (Type III vs Type II) = 25.0). Accordingly, Type III transients were much more common in infarcted tissue than the other transient types.

Oxyhemoglobin transients

The oxy-hemoglobin transients shared several similarities with the CBF transients. Of the total number of transients analyzed, 45% were in the infarcted tissue and 55% were in the non-infarcted tissue. The PAmp ($p = 0.007$) and Pslope ($p = 0.001$) parameters were higher in the non-infarcted tissue than the infarcted tissue (Table 3, Fig. 6). Note, however, that in contrast to CBF transients, the Oxy-Hb TAmplitude parameter was not associated with infarction. The other transient

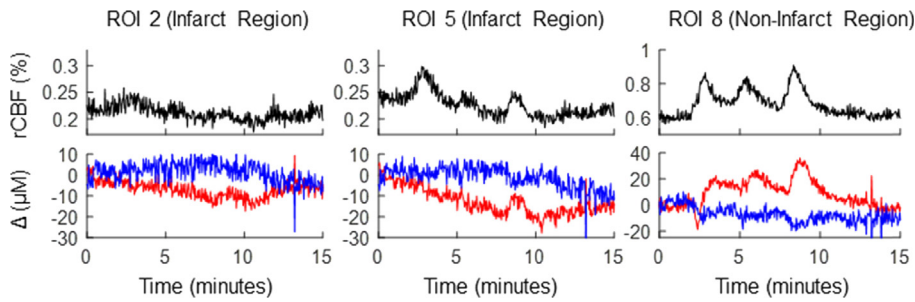


Fig. 4. Example temporal traces of relative cerebral blood flow (rCBF; top row), change in oxy-hemoglobin concentration (red curve; bottom row), and change in deoxy-hemoglobin concentration (blue curve; bottom row) at three regions of interest (ROI; as illustrated in Fig. 5, #2 and #5 are in the infarct region, #8 is in the non-infarct region) in the same animal. Time-zero is immediately after middle cerebral artery occlusion. rCBF is the percentage of the pre-occlusion CBF level, and the differential hemoglobin concentration changes (Δ) are relative to the average levels during the first minute after occlusion. Note, the vertical axis scale for ROI 8 is different from that for ROIs 2 and 5.

Table 1. Summary of the spatial distributions (% of total) for the different types of cerebral blood flow (CBF), oxy-hemoglobin (Oxy-Hb), and deoxy-hemoglobin (Deoxy-Hb) transients. The total number of CBF, Oxy-Hb, and Deoxy-Hb transients were 285, 234, and 196, respectively

TYPES	CBF	Oxy-Hb	Deoxy-Hb
INFARCTED			
I	15%	3.8%	24%
II	13%	10%	14%
III	21%	31%	7.3%
NON-INFARCTED			
I	35%	22%	29%
II	16%	29%	9.9%
III	0.7%	3.8%	17%

characterization parameters were also not associated with infarction.

Oxy-Hb transient type was associated with infarction ($p < 0.001$). The generalized mixed logistic regression model estimated that the odds of infarction for Type III are 29.8 and 20.7 times higher than the corresponding odds for Type I and Type II, respectively (i.e., OR (Type III vs Type I) = 29.8, OR (Type III vs Type II) = 20.7). Thus, as with the CBF transient type, Type III transients were more common in infarcted tissue than the other transient types.

Table 2. Summary of the descriptive statistics of the cerebral blood flow (CBF) transient characterization parameters (negative amplitude (NAmp, %), positive amplitude (PAmp, %), total amplitude (Tamp, %), duration (second), negative slope (Nslope, NAmp/second), and positive slope (Pslope, PAmp/second) are defined in Fig. 3 and in the Analysis of Transients subsection). Both the experimental mean and standard deviation, as well as the estimated mean and standard error of the estimated mean from the mixed ANOVA model, are reported. The p values are from the mixed ANOVA model comparison of infarcted to non-infarcted tissue. PAmp, TAmP and Pslope were associated with infarction

CBF		NAmp	PAmp	TAmP	Duration	NSlope	PSlope
INFARCTED	Mean	13.74	10.13	15.54	149.83	0.48	0.16
	Std. Deviation	7.32	8.56	10.86	71.85	0.33	0.15
	Estimated Mean	13.93	9.87	15.15	151.04	0.46	0.16
	Std. Error of Estimated Mean	0.98	2.11	1.78	9.89	0.04	0.04
NON-INFARCTED	Mean	11.49	31.64	34.60	183.58	0.57	0.60
	Std. Deviation	7.08	18.69	19.45	70.07	0.38	0.37
	Estimated Mean	11.41	30.10	32.85	182.73	0.54	0.58
	Std. Error of Estimated Mean	1.34	1.83	1.98	11.13	0.06	0.04
STATISTICS	p-values	0.14	<0.001	<0.001	0.07	0.32	<0.001

Deoxyhemoglobin transients

Of the total number of Deoxy-Hb transients analyzed, 45% were in the infarcted tissue and 55% were in the non-infarcted tissue. Compared to the infarcted tissue, the Pslope parameter was higher ($p = 0.007$) and the duration parameter was lower ($p < 0.001$) in the non-infarcted tissue (Table 4, Fig. 7). None of the other characterization parameters analyzed were associated with infarction. In addition, Deoxy-Hb transient type was not associated with infarction ($p = 0.5$).

DISCUSSION

Our study provides multispectral and multimodal (LSI + OIS) imaging data about the spatial distribution of both flow-and hemoglobin transients in a focal brain ischemia model of the rat. Notably, we identified several variables of these transients which distinguished injured versus non-injured territories in ischemic stroke. The transient type (I-III), and the positive slope of the transients, appear to hold particular promise for translational research of acute brain injuries. Thus, regional heterogeneity of the transients detected by optical imaging might serve as a noninvasive hemodynamic and functional biomarker of the underlying cortex.

Flow transients

We observed in 2009 that the shape of flow transients is highly diverse in rat focal cerebral ischemia (Luckl et al., 2009). Spatial trends in spreading depression related flow transients have also been observed during focal ischemia in cats (Strong et al., 2007), swine (Schöll et al., 2017), and mice (Shin et al., 2006). Although to our knowledge, such spatial trends have not yet been directly observed in humans, case examples of heterogeneous CBF responses to SDs have been detected with invasive ECoG and CBF monitoring in subarachnoid hemorrhage

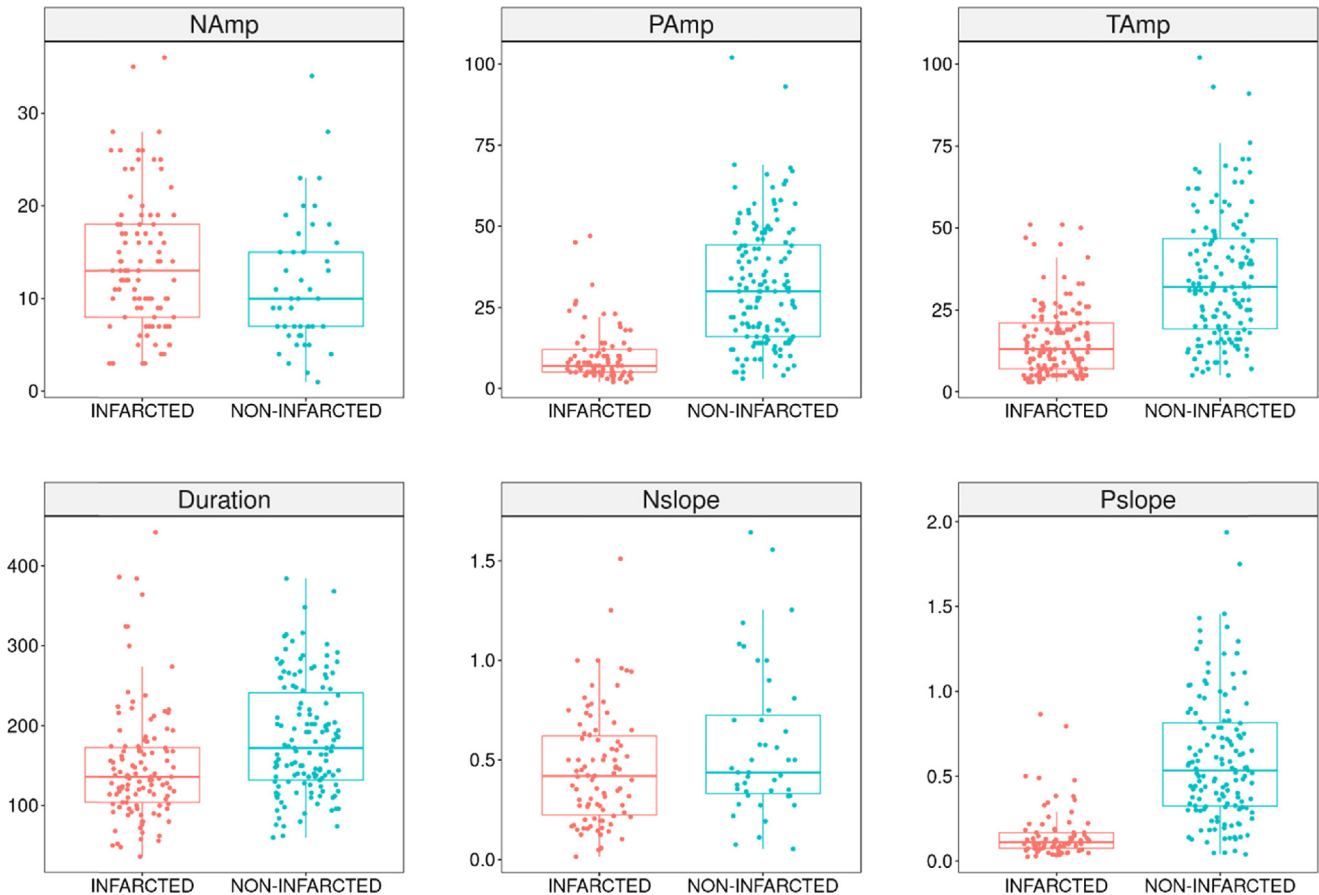


Fig. 5. Spatial distributions (INFARCTED vs NON-INFARCTED) of the different characterization parameters of the cerebral blood flow transients. Boxplots show the median and interquartile range of the characterization parameter on the vertical axis. The negative amplitude ($n = 141$) (NAmp, %), positive amplitude ($n = 226$) (PAmp, %), total amplitude ($n = 285$) (TAmp, %), duration ($n = 255$) (second), negative slope ($n = 136$) (Nslope, NAmp/second), and positive slope ($n = 220$) (Pslope, PAmp/second) are defined in Fig. 3 and in the Analysis of Transients subsection. PAmp, TAmp, and Pslope were higher in the non-infarcted tissue than the infarcted tissue ($p < 0.001$ for all three comparisons). There was no difference between non-infarcted and infarcted tissue in the other parameters.

Table 3. Summary of the descriptive statistics of the oxy-hemoglobin (Oxy-Hb) transient characterization parameters (negative amplitude (NAmp, μM), positive amplitude (PAmp, μM), total amplitude (TAmp, μM), duration (second), negative slope (Nslope, NAmp/second), and positive slope (Pslope, PAmp/second) are defined in Fig. 3 and in the Analysis of Transients subsection). Both the experimental mean and standard deviation, as well as the estimated mean and standard error of the estimated mean from the mixed ANOVA model, are reported. The p values are from the mixed ANOVA model comparison of infarcted to non-infarcted tissue. PAmp and PSlope were associated with infarction

Oxy-Hb		NAmp	PAmp	TAmp	Duration	NSlope	PSlope
INFARCTED	Mean	55.46	25.58	60.29	236.64	1.51	0.24
	Std. Deviation	38.94	17.70	42.23	122.94	1.12	0.21
	Estimated Mean	54.33	27.70	57.84	239.61	1.44	0.25
	Std. Error of Estimated Mean	5.19	7.99	6.35	14.66	0.15	0.17
NON-INFARCTED	Mean	38.70	57.12	77.10	237.77	1.78	1.04
	Std. Deviation	22.27	40.97	46.84	99.53	1.74	0.89
	Estimated Mean	39.21	55.57	75.10	235.82	1.58	0.99
	Std. Error of Estimated Mean	6.49	5.88	6.93	12.61	0.17	0.12
STATISTICS	p - values	0.14	<0.001	0.07	0.85	0.52	<0.001

patients (Dreier et al., 2009). These studies motivated us to rigorously compare spatial differences in flow transients propagating in tissue dichotomized by histological outcome. We found that hypoperfusive transients (type III) are associated mostly with the infarcted region while the hyperemic transients (type I) are characteristic for non-infarcted regions.

The continuum of hemodynamic responses to SDs encompasses transient events from hyperemia to hypoperfusion. It is known that peak hyperemia is characteristic for a healthy tissue in most species (Ayata and Lauritzen, 2015). Accordingly, we primarily observed hyperemic transients in rats over the non-injured territory with relatively higher post-occlusive CBF values. How-

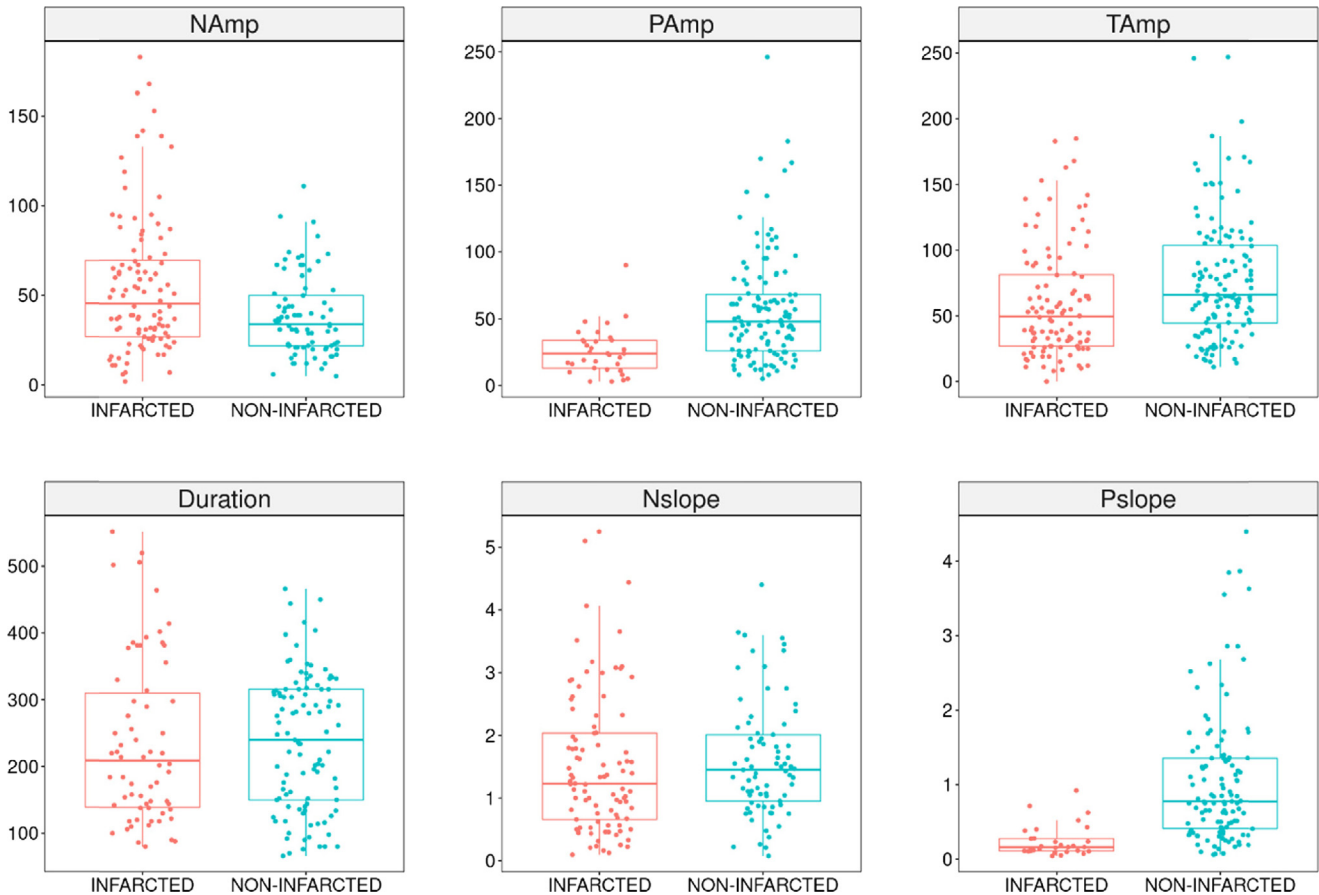


Fig. 6. Spatial distributions (INFARCTED vs NON-INFARCTED) of the different characterization parameters of the oxy-hemoglobin transients. Boxplots show the median and interquartile range of the characterization parameter on the vertical axis. The negative amplitude ($n = 185$) (NAm, μM), positive amplitude ($n = 153$) (PAmp, μM), total amplitude ($n = 234$) (TAmp, μM), duration ($n = 169$) (second), negative slope ($n = 174$) (Nslope, NAm/second), and positive slope ($n = 146$) (Pslope, PAmp/second) are defined in Fig. 3 and in the Analysis of Transients subsection. PAmp ($p = 0.007$) and Pslope ($p = 0.001$) were higher in the non-infarcted tissue than the infarcted tissue. There was no difference between non-infarcted and infarcted tissue in the other parameters.

Table 4. Summary of the descriptive statistics of the deoxy-hemoglobin (Deoxy-Hb) transient characterization parameters (negative amplitude (NAm, μM), positive amplitude (PAmp, μM), total amplitude (TAmp, μM), duration (second), negative slope (Nslope, NAm/second), and positive slope (Pslope, PAmp/second) are defined in Fig. 3 and in the Analysis of Transients subsection). Both the experimental mean and standard deviation, as well as the estimated mean and standard error of the estimated mean from the mixed ANOVA model, are reported. The p values are from the mixed ANOVA model comparison of infarcted to non-infarcted tissue. Duration and Pslope were associated with infarction

Deoxy-Hb		NAm	PAmp	TAmp	Duration	NSlope	PSlope
INFARCTED	Mean	16.41	20.76	24.43	211.74	0.59	0.29
	Std. Deviation	17.62	12.08	17.84	75.78	0.55	0.21
	Estimated Mean	16.31	20.84	24.23	211.68	0.57	0.29
	Std. Error of Estimated Mean	2.34	1.55	1.86	8.86	0.08	0.05
NON-INFARCTED	Mean	19.88	22.51	24.96	153.60	0.59	0.55
	Std. Deviation	8.99	13.22	14.96	63.58	0.32	0.48
	Estimated Mean	19.68	22.14	24.73	153.58	0.58	0.55
	Std. Error of Estimated Mean	2.25	1.62	1.77	8.44	0.08	0.05
STATISTICS	p- values	0.31	0.57	0.85	<0.001	0.92	<0.001

ever, a hypoperfusive response - a spreading ischemia – dominates the injured territories with lower post-occlusive CBF values. This inverse, hemodynamic response has been observed in a model mimicking the situation after aneurysmal subarachnoid bleeding (Dreier et al., 1998),

in which artificial cerebrospinal fluid with an elevated K⁺ concentration together with NO scavenger hemoglobin were topically applied to the cerebral cortex. Similar conditions due to elevated extracellular potassium concentration and reduced NO synthesis are likely present after

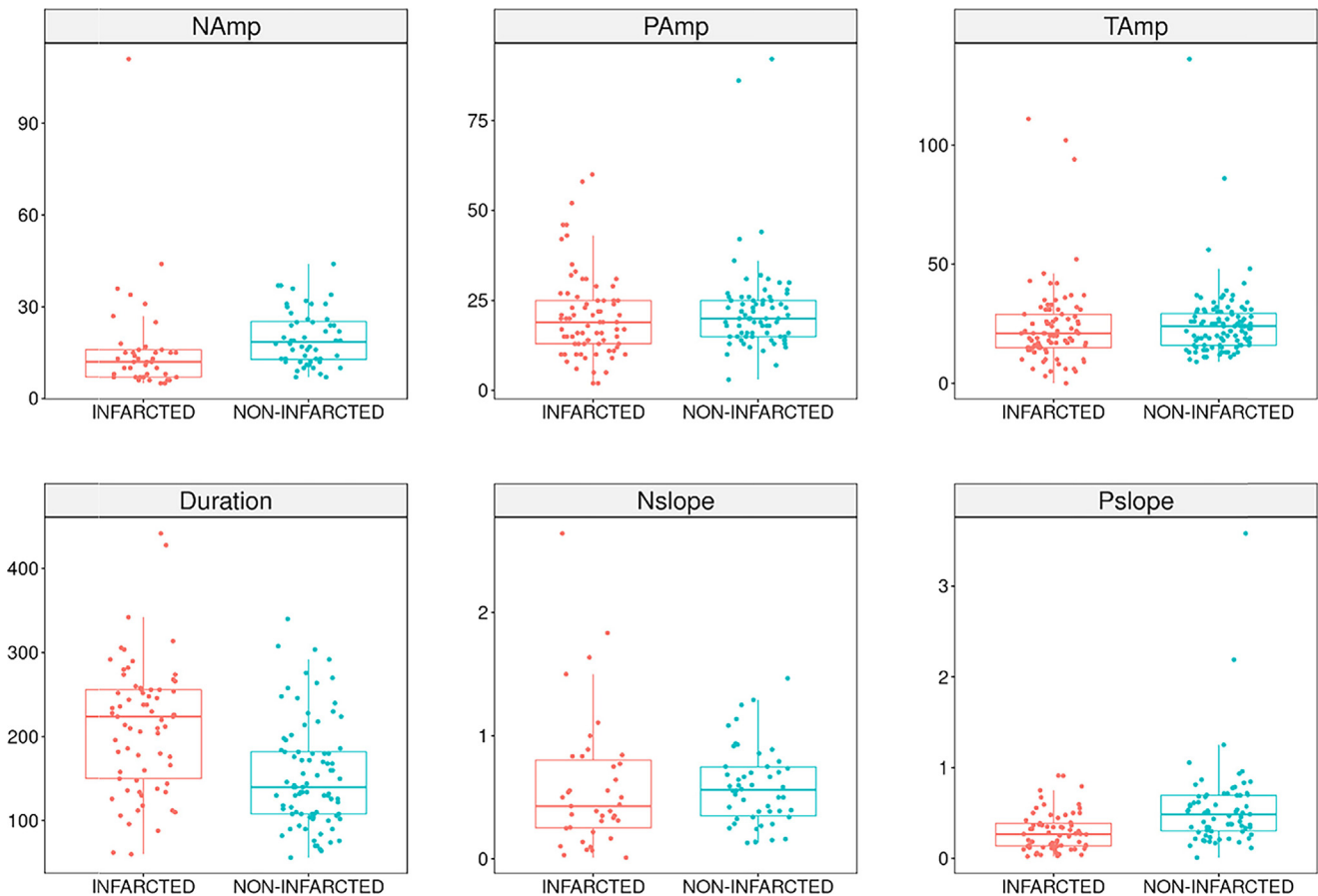


Fig. 7. Spatial distributions (INFARCTED vs NON-INFARCTED) of the different characterization parameters of the deoxy-hemoglobin transients. Boxplots show the median and interquartile range of the characterization parameter on the vertical axis. The negative amplitude ($n = 93$) (NAmp, μM), positive amplitude ($n = 150$) (PAmp, μM), total amplitude ($n = 196$) (TAmp, μM), duration ($n = 154$) (second), negative slope ($n = 89$) (Nslope, NAmp/s), and positive slope ($n = 141$) (Pslope, PAmp/second) are defined in Fig. 3 and in the Analysis of Transients subsection. Compared to the infarcted tissue, duration ($p < 0.001$) was lower and Pslope ($p = 0.007$) was higher in the non-infarcted tissue. There was no difference between non-infarcted and infarcted tissue in the other parameters.

arterial occlusion (Lemale et al., 2022). In a vicious circle, spreading ischemia further deteriorates perfusion in the underlying brain tissue.

Three out of six characterization variables of the flow transients exhibited significant spatial heterogeneity in our study. To our surprise, Pslope, proved to be an excellent indicator for viable tissue. Similarly, a positive correlation between the resting state rCBF and PSlope was observed in another rat ischemia study (Feuerstein et al., 2014). The authors considered Pslope as the functional marker of the capacity to raise CBF. The strong associations of the other two variables (PAmp, TAmp) with infarction observed herein are consistent with the findings of our prior studies that used residual blood flow after MCA occlusion as a proxy of infarction. Specifically, in rat focal brain ischemia, we identified positive correlations between the residual blood flow and the average amplitude of the positive and negative peaks of the transients (Luckl et al., 2009; Lückl et al., 2012).

Summarizing our results in context with the abundant literature of this field, we conclude that the flow transient is a good candidate for noninvasive monitoring of SDs in translational research.

Oxy- and deoxyhemoglobin transients

Analogously to the flow transients, the oxy-hemoglobin transients manifested typically as a monophasic decrease in the oxy-hemoglobin concentration (type III) over the infarcted region, while biphasic changes (type II) or monophasic increase (type I) were characteristic over the non-infarcted region. An opposite but not significant trend was observed with the deoxy-hemoglobin transients. These morphology findings are supported by a previous OIS/LSI imaging study of six mice after distal MCA occlusion (Jones et al., 2008). In this study, three regions (core, penumbra, non-ischemic) were identified based on residual CBF measurements, and oxy- and deoxy-hemoglobin transients were observed. Although histological outcome was not determined in this study, and a statistical comparison of transient morphology across regions was not done, the authors showed case examples of hemoglobin trends with similar spatial trends to those reported herein. Case examples of similar spatial patterns in total hemoglobin transients (estimated from OIS intensity images at a single wavelength) were also observed in swine and rat focal ischemia models (Bere et al., 2014; Schöll et al., 2017).

Finally, evidence of heterogeneous oxygenation responses to SDs were observed with invasive ECoG and local brain tissue oxygen tension monitoring in humans with subarachnoid hemorrhage (Winkler et al., 2017).

SD increases metabolism and oxygen demand in brain to restore ionic gradients across neuronal membranes and causes a O₂ supply–demand mismatch in brain tissue (Ayata and Lauritzen, 2015). The heterogeneity of the hemoglobin transients may reflect this mismatch. The volume of mismatch may be smaller in tissue with better perfusion and a hyperemic response to SD, and more pronounced in tissue with hypoperfusion and in the presence of spreading ischemia. Oxygen availability is an important marker in the metabolic stress. Both reduced supply due to hypoperfusion (vasoconstriction) or an increased capillary transit time heterogeneity and increased demands may alter oxygen delivery and availability during SD (Piilgaard and Lauritzen, 2009; Yuzawa et al., 2012; Ayata and Lauritzen, 2015).

Similar to the flow transients, the Pamp and the Pslope of the oxy-hemoglobin showed significant spatial trends. It is intriguing and promising that the Pslope parameter for both the oxy- and deoxy-hemoglobin transients was associated with histological outcome. We believe, that Pslope may reflect the capacity of the underlying tissue to respond to metabolic demand. Surprisingly, in contrast to the flow and oxy-hemoglobin transients, the deoxy-hemoglobin transient duration was also associated with infarction. This result, however, should be interpreted carefully. There is less statistical power in the duration comparisons because the duration could not be determined for 28% and 21% of the detected oxy-hemoglobin and deoxy-hemoglobin transients, respectively. As described above, duration could not be determined for transients that did not return to the pre-transient baseline level at all (more details about transients with this feature are described elsewhere (Luckl et al., 2009)) or for transients that did not return to baseline by the end of the 15-min long sequence of LSI/OIS acquisition.

Of note, the flow transients appear to exhibit a stronger association with infarction than do the oxy-hemoglobin and deoxy-hemoglobin transients. This may be partly due to the LSI measurements being less noisy than the OIS measurements, and partly due to the reduced number of hemoglobin transients detected. As described in the results section, one reason for the smaller number of hemoglobin transients is OIS instrumentation malfunction. Future study is needed to understand the other reasons. Possibly, the spatial extent (area) of the propagating oxy-hemoglobin and deoxy-hemoglobin transients is smaller than that of the flow transients. If this is the case, the circular ROIs (see Fig. 2) could have captured some flow transients that were bypassed by hemoglobin transients.

Aspects of the translational research

The mechanisms eliciting SDs are very complex. Cerebral ischemia depolarizes neurons indirectly by the Na⁺/K⁺ ATP-ase activity reduction (Somjen, 2001).

The channels that initiate or terminate/regenerate SDs have been heavily studied and discussed in the literature (Czéh et al., 1992; Van Dusen et al., 2020; Andrew et al., 2022; Shayan et al., 2022) but are still not clearly identified. Besides ischemia, products of hemolysis (Dreier et al., 2000), mechanical stretch from hematoma growth (Fischer et al., 2021), cortical shear stress from concussive TBI (Bouley et al., 2019), and intracranial pressure spikes (Oka et al., 2022) can also elicit SDs. In addition, there are well known “aggravating” factors such as hyperthermia (Hartings et al., 2009), hypoxia and hypotension (von Bornstädt et al., 2015) that can further trigger SDs. SD triggers can be present in different combinations in patients with acute brain injury. For example, a febrile patient with subarachnoid hemorrhage (hemolysis), hematoma (mechanical stretch) and vasospasm (ischemia) likely experiences SDs arising from many triggers.

Different variables of SDs have proven to be good predictors for outcome in studies of traumatic brain injuries (Hartings et al., 2011) and subarachnoid hemorrhage (Luckl et al., 2018; Eriksen et al., 2019). ECoG is still the gold standard for detection of SD. Nevertheless, this invasive, neurophysiological recording does not permit the monitoring of patients who do not need to undergo craniotomy. Accordingly, the use of non-invasive technologies for monitoring is preferred (Dreier et al., 2017).

To this end, the use of continuous scalp EEG has been investigated. In two different COSBID studies, SDs manifested in the scalp EEG signals as depressions of ongoing activity (Drenckhahn et al., 2012; Hartings et al., 2014). However, Hofmeijer and colleagues were unable to identify univocal characteristics of SD with full band scalp EEG in patients with cerebral ischemia or traumatic brain injury (Hofmeijer et al., 2018)⁴⁴. EEG also failed to detect SDs reliably on the scalp in our rat focal ischemia study (unpublished data).

One explanation for these conflicting findings might be that the COSBID patients all underwent neurosurgery to treat their injuries, while the skull was intact for the patients in the other study. The removal of the skull, which serves as a filter, might elucidate why the COSBID studies yielded positive results. It's also possible that differences in methodology used in the study with intact skulls (e.g., visual EEG-review only in 1-h blocks) could have precluded detection of SD induced EEG depression. In addition, the use of high-density EEG has been proposed for the detection of SDs over the scalp (Chamanzar et al., 2019; Hund et al., 2022), though the clinical feasibility of such measurements is questionable.

Our results support the clinical relevance of monitoring SD-related flow and hemoglobin transients for ischemic stroke patients. To this end, the non-invasive optical techniques of diffuse correlation spectroscopy and near-infrared spectroscopy are promising for translation. One possible translational roadblock is that DCS and NIRS have lower spatial resolutions than laser speckle and OIS. High-density NIRS systems can achieve cortical spatial resolutions of ~ 1 cm (Wheelock et al., 2019). This resolution should

still be high enough, though, to detect SDs (Hund et al., 2022). Important future work is needed to assess whether optical imaging alone or in combination with other methods (for example EEG) is suitable to detect SDs non-invasively.

Study limitations

Our study has limitations. One possible confound is anesthesia. We do not think-however-that anesthesia impacts the main findings of our study. Previous ischemia studies with different species (mouse, rat, cat, swine) and using different anesthetics (isoflurane, halothane, chloralose, propofol, midazolam) report a similar regional heterogeneity of the types of the transients (CBF, OIS signal)(Shin et al., 2006; Strong et al., 2007; Luckl et al., 2009; Bere et al., 2014; Schöll et al., 2017). In addition, heterogeneous oxygenation responses to SDs were detected with invasive ECoG and local brain tissue oxygen tension monitoring in patients with subarachnoid haemorrhage (Winkler et al., 2017). Some differences in the length or in the amplitude of the transients might be possible, however no data examining this has been obtained. Regrettable OIS instrumentation malfunction for some of the data acquisition is another limitation. This might have contributed to the lower number of detected hemoglobin transients than flow transients. Finally, as we noted above, laser speckle and OIS techniques can't be used non-invasively in humans, but diffuse correlation spectroscopy (DCS) and near-infrared spectroscopy (NIRS) techniques, which measure the same contrasts, can be used.

CONCLUSIONS

Our study identified many variables of flow and hemoglobin transients which can distinguish infarcted versus non-infarcted areas in a rat model of ischemic stroke. Interestingly, Pslope was the only variable found to be associated with infarction in all three transient contrasts (i.e., flow, oxy-hemoglobin, deoxy-hemoglobin). The results suggest that noninvasive optical imaging, in combination with scalp EEG, could help meet the great need for transcranial detection of SDs. The information from routine, bedside monitoring of SDs could also enable personalized neuroprotection before the brain injury becomes irreversible.

ACKNOWLEDGMENTS

This study was supported by National Institutes of Health grant NS057400.

REFERENCES

Andrew RD, Hartings JA, Ayata C, Brennan KC, Dawson-Scully KD, Farkas E, Herreras O, Kirov SA, Müller M, Ollen-Bittle N, Reiffurth C, Revah O, Robertson RM, Shuttleworth CW, Ullah G, Dreier JP (2022) The critical role of spreading depolarizations in early brain injury: consensus and contention. *Neurocrit Care* 37:83–101.

Ayata C, Lauritzen M (2015) Spreading depression, spreading depolarizations, and the cerebral vasculature. *Physiol Rev* 95:953–993.

Baker WB, Sun Z, Hiraki T, Putt ME, Durduran T, Reivich M, Yodh AG, Greenberg JH (2013) Neurovascular coupling varies with level of global cerebral ischemia in a rat model. *J Cereb Blood Flow Metab* 33:97–105.

Bardutzky J, Shen Q, Henninger N, Bouley J, Duong TQ, Fisher M (2005) Differences in ischemic lesion evolution in different rat strains using diffusion and perfusion imaging. *Stroke* 36:2000–2005.

Bederson JB, Pitts LH, Germano SM, Nishimura MC, Davis RL, Bartkowski HM (1986) Evaluation of 2,3,5-triphenyltetrazolium chloride as a stain for detection and quantification of experimental cerebral infarction in rats. *Stroke* 17:1304–1308.

Bere Z, Obrenovitch TP, Kozák G, Bari F, Farkas E (2014) Imaging reveals the focal area of spreading depolarizations and a variety of hemodynamic responses in a rat microembolic stroke model. *J Cereb Blood Flow Metab* 34:1695–1705.

Bouley J, Chung DY, Ayata C, Brown Jr RH, Henninger N (2019) Cortical Spreading Depression Denotes Concussion Injury. *J Neurotrauma* 36:1008–1017.

Briers JD (2001) Laser Doppler, speckle and related techniques for blood perfusion mapping and imaging. *Physiol Meas* 22: R35–R66.

Brown H, Prescott R (1999) Applied mixed models in medicine. Chichester UK: Wiley.

Chamanzar A, George S, Venkatesh P, Chamanzar M, Shutter L, Elmer J, Grover P (2019) An Algorithm for Automated, Noninvasive Detection of Cortical Spreading Depolarizations Based on EEG Simulations. *IEEE Trans Biomed Eng* 66:1115–1126.

Chuquet J, Hollender L, Nimchinsky EA (2007) High-resolution in vivo imaging of the neurovascular unit during spreading depression. *J Neurosci* 27:4036–4044.

Czéh G, Aitken PG, Somjen GG (1992) Whole-cell membrane current and membrane resistance during hypoxic spreading depression. *Neuroreport* 3:197–200.

Czeh G, Aitken PG, Somjen GG (1993) Membrane currents in CA1 pyramidal cells during spreading depression (SD) and SD-like hypoxic depolarization. *Brain Res* 632:195–208.

Dahlem MA, Müller SC (1997) Self-induced splitting of spiral-shaped spreading depression waves in chicken retina. *Exp Brain Res* 115:319–324.

Dohmen C, Sakowitz OW, Fabricius M, Bosche B, Reithmeier T, Ernestus RI, Brinker G, Dreier JP, Woitzik J, Strong AJ, Graf R (2008) Spreading depolarizations occur in human ischemic stroke with high incidence. *Ann Neurol* 63:720–728.

Dreier JP (2011) The role of spreading depression, spreading depolarization and spreading ischemia in neurological disease. *Nat Med* 17:439–447.

Dreier JP, Körner K, Ebert N, Görner A, Rubin I, Back T, Lindauer U, Wolf T, Villringer A, Einhäupl KM, Lauritzen M, Dirnagl U (1998) Nitric oxide scavenging by hemoglobin or nitric oxide synthase inhibition by N-nitro-L-arginine induces cortical spreading ischemia when K⁺ is increased in the subarachnoid space. *J Cereb Blood Flow Metab* 18:978–990.

Dreier JP, Ebert N, Priller J, Megow D, Lindauer U, Klee R, Reuter U, Imai Y, Einhäupl KM, Victorov I, Dirnagl U (2000) Products of hemolysis in the subarachnoid space inducing spreading ischemia in the cortex and focal necrosis in rats: a model for delayed ischemic neurological deficits after subarachnoid hemorrhage? *J Neurosurg* 93:658–666.

Dreier JP, Major S, Manning A, Woitzik J, Drenckhahn C, Steinbrink J, Tolia C, Oliveira-Ferreira AI, Fabricius M, Hartings JA, Vajkoczy P, Lauritzen M, Dirnagl U, Bohner G, Strong AJ (2009) Cortical spreading ischaemia is a novel process involved in ischaemic damage in patients with aneurysmal subarachnoid haemorrhage. *Brain* 132:1866–1881.

Dreier JP, Fabricius M, Ayata C, Sakowitz OW, Shuttleworth CW, Dohmen C, Graf R, Vajkoczy P, Helbok R, Suzuki M, Schiefecker AJ, Major S, Winkler MK, Kang EJ, Milakara D, Oliveira-Ferreira AI, Reiffurth C, Revankar GS, Sugimoto K, Dengler NF, Hecht N, Foreman B, Feyen B, Kondziella D, Friberg CK, Piilgaard H,

- Rosenthal ES, Westover MB, Maslarova A, Santos E, Hertle D, Sánchez-Porras R, Jewell SL, Balança B, Platz J, Hinzman JM, Lückl J, Schoknecht K, Schöll M, Drenckhahn C, Feuerstein D, Eriksen N, Horst V, Bretz JS, Jahnke P, Scheel M, Bohner G, Rostrup E, Pakkenberg B, Heinemann U, Claassen J, Carlson AP, Kowoll CM, Lublinsky S, Chassidim Y, Shelef I, Friedman A, Brinker G, Reiner M, Kirov SA, Andrew RD, Farkas E, Güresir E, Vatter H, Chung LS, Brennan KC, Lieutaud T, Marinesco S, Maas AI, Sahuquillo J, Dahlem MA, Richter F, Herreras O, Boutelle MG, Okonkwo DO, Bullock MR, Witte OW, Martus P, van den Maagdenberg AM, Ferrari MD, Dijkhuizen RM, Shutter LA, Andaluz N, Schulte AP, MacVicar B, Watanabe T, Woitzik J, Lauritzen M, Strong AJ, Hartings JA (2017) Recording, analysis, and interpretation of spreading depolarizations in neurointensive care: Review and recommendations of the COSBID research group. *J Cereb Blood Flow Metab* 37:1595–1625.
- Dreier JP, Winkler MKL, Major S, Horst V, Lublinsky S, Kola V, Lemale CL, Kang EJ, Maslarova A, Salur I, Lückl J, Platz J, Jorks D, Oliveira-Ferreira AI, Schoknecht K, Reiffurth C, Milakara D, Wiesenthal D, Hecht N, Dengler NF, Liotta A, Wolf S, Kowoll CM, Schulte AP, Santos E, Güresir E, Unterberg AW, Sarrafzadeh A, Sakowitz OW, Vatter H, Reiner M, Brinker G, Dohmen C, Shelef I, Bohner G, Scheel M, Vajkoczy P, Hartings JA, Friedman A, Martus P, Woitzik J (2022) Spreading depolarizations in ischaemia after subarachnoid haemorrhage, a diagnostic phase III study. *Brain*.
- Drenckhahn C, Winkler MK, Major S, Scheel M, Kang EJ, Pinczolis A, Grozea C, Hartings JA, Woitzik J, Dreier JP (2012) Correlates of spreading depolarization in human scalp electroencephalography. *Brain* 135:853–868.
- Dunn AK, Bolay H, Moskowitz MA, Boas DA (2001) Dynamic imaging of cerebral blood flow using laser speckle. *J Cereb Blood Flow Metab* 21:195–201.
- Dunn AK, Devor A, Bolay H, Andermann ML, Moskowitz MA, Dale AM, Boas DA (2003) Simultaneous imaging of total cerebral hemoglobin concentration, oxygenation, and blood flow during functional activation. *Opt Lett* 28:28–30.
- Durduran T, Burnett MG, Yu G, Zhou C, Furuya D, Yodh AG, Detre JA, Greenberg JH (2004) Spatiotemporal quantification of cerebral blood flow during functional activation in rat somatosensory cortex using laser-speckle flowmetry. *J Cereb Blood Flow Metab* 24:518–525.
- Eriksen N, Rostrup E, Fabricius M, Scheel M, Major S, Winkler MKL, Bohner G, Santos E, Sakowitz OW, Kola V, Reiffurth C, Hartings JA, Vajkoczy P, Woitzik J, Martus P, Lauritzen M, Pakkenberg B, Dreier JP (2019) Early focal brain injury after subarachnoid hemorrhage correlates with spreading depolarizations. *Neurology* 92:e326–e341.
- Feuerstein D, Takagaki M, Gramer M, Manning A, Endepols H, Vollmar S, Yoshimine T, Strong AJ, Graf R, Backes H (2014) Detecting tissue deterioration after brain injury: regional blood flow level versus capacity to raise blood flow. *J Cereb Blood Flow Metab* 34:1117–1127.
- Fischer P, Sugimoto K, Chung DY, Tamim I, Morais A, Takizawa T, Qin T, Gomez CA, Schlunk F, Endres M, Yaseen MA, Sakadzic S, Ayata C (2021) Rapid hematoma growth triggers spreading depolarizations in experimental intracortical hemorrhage. *J Cereb Blood Flow Metab* 41:1264–1276.
- Grinvald A, Lieke E, Frostig RD, Gilbert CD, Wiesel TN (1986a) Functional architecture of cortex revealed by optical imaging of intrinsic signals. *Nature* 324:361–364.
- Grinvald A, Segal M, Kuhnt U, Hildesheim R, Manker A, Anglister L, Freeman JA (1986b) Real-time optical mapping of neuronal activity in vertebrate CNS in vitro and in vivo. *Soc Gen Physiol Ser* 40:165–197.
- Hartings JA, Strong AJ, Fabricius M, Manning A, Bhatia R, Dreier JP, Mazzeo AT, Tortella FC, Bullock MR (2009) Spreading depolarizations and late secondary insults after traumatic brain injury. *J Neurotrauma* 26:1857–1866.
- Hartings JA, Bullock MR, Okonkwo DO, Murray LS, Murray GD, Fabricius M, Maas AI, Woitzik J, Sakowitz O, Mathern B, Roozenbeek B, Lingsma H, Dreier JP, Puccio AM, Shutter LA, Pahl C, Strong AJ (2011) Spreading depolarisations and outcome after traumatic brain injury: a prospective observational study. *Lancet Neurol* 10:1058–1064.
- Hartings JA, Wilson JA, Hinzman JM, Pollandt S, Dreier JP, DiNapoli V, Ficker DM, Shutter LA, Andaluz N (2014) Spreading depression in continuous electroencephalography of brain trauma. *Ann Neurol* 76:681–694.
- Hartings JA, Shuttleworth CW, Kirov SA, Ayata C, Hinzman JM, Foreman B, Andrew RD, Boutelle MG, Brennan KC, Carlson AP, Dahlem MA, Drenckhahn C, Dohmen C, Fabricius M, Farkas E, Feuerstein D, Graf R, Helbok R, Lauritzen M, Major S, Oliveira-Ferreira AI, Richter F, Rosenthal ES, Sakowitz OW, Sánchez-Porras R, Santos E, Schöll M, Strong AJ, Urbach A, Westover MB, Winkler MK, Witte OW, Woitzik J, Dreier JP (2017) The continuum of spreading depolarizations in acute cortical lesion development: Examining Leão's legacy. *J Cereb Blood Flow Metab* 37:1571–1594.
- Hofmeijer J, van Kaam CR, van de Werff B, Vermeer SE, Tjepkema-Cloostermans MC, van Putten M (2018) Detecting Cortical Spreading Depolarization with Full Band Scalp Electroencephalography: An Illusion? *Front Neurol* 9:17.
- Hossmann KA (1996) Perinfarct depolarizations. *Cerebrovasc Brain Metab Rev* 8:195–208.
- Hund SJ, Brown BR, Lemale CL, Menon PG, Easley KA, Dreier JP, Jones SC (2022) Numerical Simulation of Concussive-Generated Cortical Spreading Depolarization to Optimize DC-EEG Electrode Spacing for Noninvasive Visual Detection. *Neurocrit Care*.
- Jander S, Schroeter M, Peters O, Witte OW, Stoll G (2001) Cortical spreading depression induces proinflammatory cytokine gene expression in the rat brain. *J Cereb Blood Flow Metab* 21:218–225.
- Jones M, Berwick J, Johnston D, Mayhew J (2001) Concurrent optical imaging spectroscopy and laser-Doppler flowmetry: the relationship between blood flow, oxygenation, and volume in rodent barrel cortex. *Neuroimage* 13:1002–1015.
- Jones PB, Shin HK, Boas DA, Hyman BT, Moskowitz MA, Ayata C, Dunn AK (2008) Simultaneous multispectral reflectance imaging and laser speckle flowmetry of cerebral blood flow and oxygen metabolism in focal cerebral ischemia. *J Biomed Opt* 13 044007.
- Kohl M, Lindauer U, Rojl G, Kuhl M, Gold L, Villringer A, Dirnagl U (2000) Physical model for the spectroscopic analysis of cortical intrinsic optical signals. *Phys Med Biol* 45:3749–3764.
- Largo C, Cuevas P, Somjen GG, Martín del Río R, Herreras O (1996) The effect of depressing glial function in rat brain in situ on ion homeostasis, synaptic transmission, and neuron survival. *J Neurosci* 16:1219–1229.
- Lauritzen M, Dreier JP, Fabricius M, Hartings JA, Graf R, Strong AJ (2011) Clinical relevance of cortical spreading depression in neurological disorders: migraine, malignant stroke, subarachnoid and intracranial hemorrhage, and traumatic brain injury. *J Cereb Blood Flow Metab* 31:17–35.
- Leao AA (1944) Spreading depression of activity in the cerebral cortex. *J Neurophysiol* 7:359–390.
- Lemale CL, Lückl J, Horst V, Reiffurth C, Major S, Hecht N, Woitzik J, Dreier JP (2022) Migraine Aura, Transient Ischemic Attacks, Stroke, and Dying of the Brain Share the Same Key Pathophysiological Process in Neurons Driven by Gibbs-Donnan Forces, Namely Spreading Depolarization. *Front Cell Neurosci* 16 837650.
- Luckl J, Keating J, Greenberg JH (2008) Alpha-chloralose is a suitable anesthetic for chronic focal cerebral ischemia studies in the rat: a comparative study. *Brain Res* 1191:157–167.
- Luckl J, Zhou C, Durduran T, Yodh AG, Greenberg JH (2009) Characterization of perinfarct flow transients with laser speckle and Doppler after middle cerebral artery occlusion in the rat. *J Neurosci Res* 87:1219–1229.
- Luckl J, Baker W, Sun ZH, Durduran T, Yodh AG, Greenberg JH (2010) The biological effect of contralateral forepaw stimulation in rat focal cerebral ischemia: a multispectral optical imaging study. *Front Neuroenergetics* 2.

- Lückl J, Dreier JP, Szabados T, Wiesenthal D, Bari F, Greenberg JH (2012) Peri-infarct flow transients predict outcome in rat focal brain ischemia. *Neuroscience* 226:197–207.
- Lückl J, Lemale CL, Kola V, Horst V, Khojasteh U, Oliveira-Ferreira AI, Major S, Winkler MKL, Kang EJ, Schoknecht K, Martus P, Hartings JA, Woitzik J, Dreier JP (2018) The negative ultraslow potential, electrophysiological correlate of infarction in the human cortex. *Brain* 141:1734–1752.
- Nicholson C, Kraig RP, ten Bruggencate G, Stöckle H, Steinberg R (1978) Potassium, calcium, chloride and sodium changes in extracellular space during spreading depression in cerebellum [proceedings]. *Arzneimittelforschung* 28:874–875.
- O'Brien TP, Chen S, Farkas E (2009) Simultaneous, live imaging of cortical spreading depression and associated cerebral blood flow changes, by combining voltage-sensitive dye and laser speckle contrast methods. *Neuroimage* 45:68–74.
- Oka F, Sadeghian H, Yaseen MA, Fu B, Kura S, Qin T, Sakadžić S, Sugimoto K, Inoue T, Ishihara H, Nomura S, Suzuki M, Ayata C (2022) Intracranial pressure spikes trigger spreading depolarizations. *Brain* 145:194–207.
- Parthasarathy AB, Tom WJ, Gopal A, Zhang X, Dunn AK (2008) Robust flow measurement with multi-exposure speckle imaging. *Opt Express* 16:1975–1989.
- Peixoto NL, Fernandes de Lima VM, Hanke W (2001) Correlation of the electrical and intrinsic optical signals in the chicken spreading depression phenomenon. *Neurosci Lett* 299:89–92.
- Peters O, Schipke CG, Hashimoto Y, Kettenmann H (2003) Different mechanisms promote astrocyte Ca²⁺ waves and spreading depression in the mouse neocortex. *J Neurosci* 23:9888–9896.
- Piilgaard H, Lauritzen M (2009) Persistent increase in oxygen consumption and impaired neurovascular coupling after spreading depression in rat neocortex. *J Cereb Blood Flow Metab* 29:1517–1527.
- Risher WC, Andrew RD, Kirov SA (2009) Real-time passive volume responses of astrocytes to acute osmotic and ischemic stress in cortical slices and in vivo revealed by two-photon microscopy. *Glia* 57:207–221.
- Schöll MJ, Santos E, Sanchez-Porras R, Kentar M, Gramer M, Silos H, Zheng Z, Gang Y, Strong AJ, Graf R, Unterberg A, Sakowitz OW, Dickhaus H (2017) Large field-of-view movement-compensated intrinsic optical signal imaging for the characterization of the haemodynamic response to spreading depolarizations in large gyrencephalic brains. *J Cereb Blood Flow Metab* 37:1706–1719.
- Shayan M, Eslami F, Amanlou A, Solaimanian S, Rahimi N, Rashidian A, Ejtemaei-Mehr S, Ghasemi M, Dehpour AR (2022) Neuroprotective effects of Lasmiditan and Sumatriptan in an experimental model of post-stroke seizure in mice: Higher effects with concurrent opioid receptors or K(ATP) channels inhibitors. *Toxicol Appl Pharmacol* 454 116254.
- Shin HK, Dunn AK, Jones PB, Boas DA, Moskowitz MA, Ayata C (2006) Vasoconstrictive neurovascular coupling during focal ischemic depolarizations. *J Cereb Blood Flow Metab* 26:1018–1030.
- Somjen GG (2001) Mechanisms of spreading depression and hypoxic spreading depression-like depolarization. *Physiol Rev* 81:1065–1096.
- Strong AJ, Anderson PJ, Watts HR, Virley DJ, Lloyd A, Irving EA, Nagafuji T, Ninomiya M, Nakamura H, Dunn AK, Graf R (2007) Peri-infarct depolarizations lead to loss of perfusion in ischaemic gyrencephalic cerebral cortex. *Brain* 130:995–1008.
- Takano T, Tian GF, Peng W, Lou N, Lovatt D, Hansen AJ, Kasischke KA, Nedergaard M (2007) Cortical spreading depression causes and coincides with tissue hypoxia. *Nat Neurosci* 10:754–762.
- Urbach A, Brueckner J, Witte OW (2015) Cortical spreading depolarization stimulates gliogenesis in the rat entorhinal cortex. *J Cereb Blood Flow Metab* 35:576–582.
- Van Dusen RA, Shuster-Hyman H, Robertson RM (2020) Inhibition of ATP-sensitive potassium channels exacerbates anoxic coma in *Locusta migratoria*. *J Neurophysiol* 124:1754–1765.
- von Bornstädt D, Houben T, Seidel JL, Zheng Y, Dilekoz E, Qin T, Sandow N, Kura S, Eikermann-Haerter K, Endres M, Boas DA, Moskowitz MA, Lo EH, Dreier JP, Woitzik J, Sakadžić S, Ayata C (2015) Supply-demand mismatch transients in susceptible peri-infarct hot zones explain the origins of spreading injury depolarizations. *Neuron* 85:1117–1131.
- Walsh JG, Muruve DA, Power C (2014) Inflammasomes in the CNS. *Nat Rev Neurosci* 15:84–97.
- Wheelock MD, Culver JP, Eggebrecht AT (2019) High-density diffuse optical tomography for imaging human brain function. *Rev Sci Instrum* 90 051101.
- Winkler MK, Dengler N, Hecht N, Hartings JA, Kang EJ, Major S, Martus P, Vajkoczy P, Woitzik J, Dreier JP (2017) Oxygen availability and spreading depolarizations provide complementary prognostic information in neuromonitoring of aneurysmal subarachnoid hemorrhage patients. *J Cereb Blood Flow Metab* 37:1841–1856.
- Yuzawa I, Sakadžić S, Srinivasan VJ, Shin HK, Eikermann-Haerter K, Boas DA, Ayata C (2012) Cortical spreading depression impairs oxygen delivery and metabolism in mice. *J Cereb Blood Flow Metab* 32:376–386.
- Zhou C, Shimazu T, Durduran T, Luckl J, Kimberg DY, Yu G, Chen XH, Detre JA, Yodh AG, Greenberg JH (2008) Acute functional recovery of cerebral blood flow after forebrain ischemia in rat. *J Cereb Blood Flow Metab* 28:1275–1284.

(Received 21 August 2022, Accepted 23 November 2022)
(Available online 29 November 2022)